

Discovery of Checkpoint Kinase Inhibitor (S)-5-(3-Fluorophenyl)-N-(piperidin-3-yl)-3-ureidothiophene-2-carboxamide (AZD7762) by Structure-Based Design and Optimization of Thiophenecarboxamide Ureas

Vibha Oza,^{*,†} Susan Ashwell,[†] Lysie Almeida,[†] Patrick Brassil,[†] Jason Breed,[‡] Chun Deng,^{†,×} Thomas Gero,[†] Michael Grondine,[†] Candice Horn,^{†,#} Stephanos Ioannidis,[†] Dongfang Liu,^{†,○} Paul Lyne,[†] Nicholas Newcombe,[‡] Martin Pass,[‡] Jon Read,[‡] Shannon Ready,^{†,∞} Siân Rowsell,[§] Mei Su,[†] Dorin Toader,[†] Melissa Vasbinder,[†] Dingwei Yu,[†] Yan Yu,[†] Yafeng Xue,^{||} Sonya Zabłudoff,^{†,●} and James Janetka^{†,⊥}

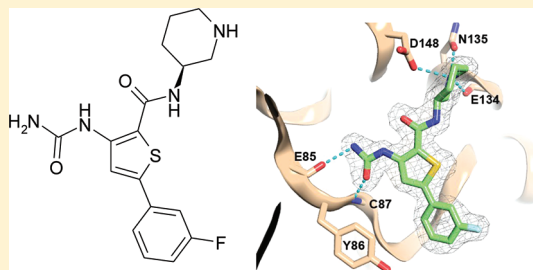
[†]AstraZeneca R&D Boston, 35 Gatehouse Drive, Waltham, Massachusetts 02451, United States

[‡]AstraZeneca R&D Alderley Park, Cheshire, SK10 4TG, United Kingdom

[§]AstraZeneca R&D, Macclesfield SK10 2NA, United Kingdom

^{||}AstraZeneca R&D Mölndal, SE-43183 Mölndal, Sweden

ABSTRACT: Checkpoint kinases CHK1 and CHK2 are activated in response to DNA damage that results in cell cycle arrest, allowing sufficient time for DNA repair. Agents that lead to abrogation of such checkpoints have potential to increase the efficacy of such compounds as chemo- and radiotherapies. Thiophenecarboxamide ureas (TCUs) were identified as inhibitors of CHK1 by high throughput screening. A structure-based approach is described using crystal structures of JNK1 and CHK1 in complex with **1** and **2** and of the CHK1–**3b** complex. The ribose binding pocket of CHK1 was targeted to generate inhibitors with excellent cellular potency and selectivity over CDK1 and IKK β , key features lacking from the initial compounds. Optimization of **3b** resulted in the identification of a regioisomeric 3-TCU lead **12a**. Optimization of **12a** led to the discovery of the clinical candidate **4** (AZD7762), which strongly potentiates the efficacy of a variety of DNA-damaging agents in preclinical models.



INTRODUCTION

The checkpoint kinases CHK1 and CHK2 play a key role in the modulation of cell cycle checkpoints to ensure the integrity of genetic information transfer and function during cell-cycle progression and DNA repair following DNA damage. CHK1 and CHK2 are structurally related Ser/Thr protein kinases that are phosphorylated by ATM and/or ATR kinases following DNA damage. Subsequent downstream phosphorylation events ultimately result in cell-cycle arrest. Inhibition of the checkpoint kinases, in particular CHK1, has been shown to abrogate DNA damage induced cell cycle arrest, allowing cells to advance through the cell cycle without repairing DNA damage leading to mitotic catastrophe and cell death or apoptosis.¹ Tumor cells are more sensitive to combination treatment with a DNA damaging agent (chemo- or radiotherapy) and a CHK1 inhibitor compared to normal cells because of the propensity of tumor cells to have genetic alterations in DNA damage signaling and repair (DDR), such as p53 mutations, which make the tumor cells more dependent on the remaining DDR machinery.² Thus, abrogation of these checkpoints is hypothesized to lead to an increased and selective killing of

tumor cells over normal cells in the context of DNA damage, and CHK1 inhibitors are highly sought after for use as chemo or radiopotentiating agents. UCN-01 represents the first example of CHK1 inhibitor.^{3a} However, in addition to CHK1, it hits a number of other kinases including PKC, CDK1, and CDK2. Because of the toxicity of UCN-01 ascribed to its polypharmacology, as well as unfavorable pharmacokinetic properties, the design and synthesis of many small molecule CHK1 selective inhibitors have been undertaken by a large number of research groups including ours.³ Culmination of these efforts has been identification of several clinical candidates in the area, namely, PF-477736, SCH-90077, XL-844, and LY2606368 to name a few.³ⁿ In the publication, we describe structure guided efforts toward optimization of a TCU class of CHK1 inhibitors to identify AZD7762.

Received: January 6, 2012

Published: May 2, 2012

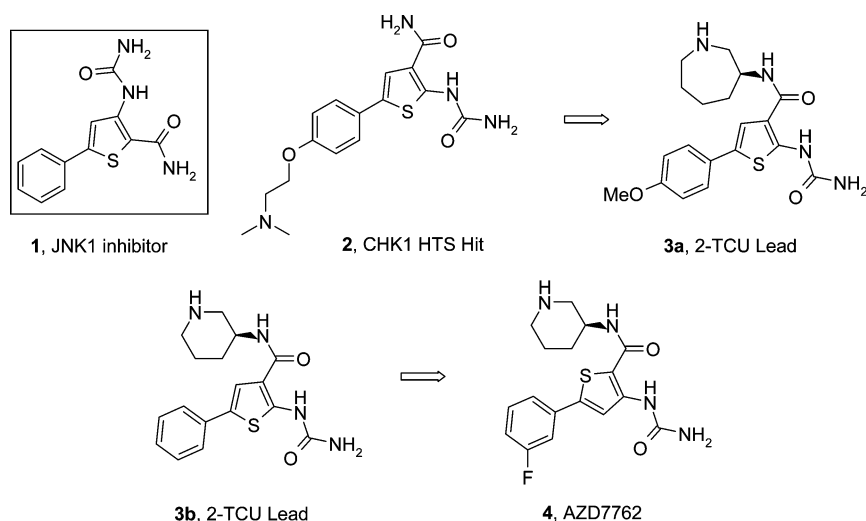


Figure 1. Evolution of the TCU class of checkpoint kinase inhibitors.

RESULTS AND DISCUSSION

In a prior communication, we reported preliminary results on the discovery and SAR of the thiophenecarboxamide urea (TCU) class of checkpoint kinase inhibitors.^{3b} In the present report, we explain in detail our X-ray crystal structure guided approach, which resulted in the rational design of lead compounds **3a** and **3b**. We further describe the lead optimization of 2-TCU **3b**, resulting in the discovery of a new class of isomeric thiophene checkpoint kinase inhibitors and the final selection of the optimized clinical candidate 3-TCU **4** (Figure 1).

X-ray Crystal Structure-Guided Identification of Lead Compound 3. TCUs have been previously described as potent ATP-competitive IKK β inhibitors.⁴ We solved an X-ray crystal structure of TCU **1** bound to JNK1, which has been used as a surrogate for IKK β which shows three atoms of the inhibitor, namely, the amide carbonyl, amide NH, and distal urea NH, making hydrogen bonds to the hinge region (Figure 2a, Table 1). We subsequently found that the TCU class of kinase inhibitors adopts a unique binding mode in CHK1. Approximately 70 compounds binding to CHK1 kinase are deposited in the Protein Data Bank. Most bind in the ATP binding site and form interactions with hinge, and some extend into the sugar pocket. Other compounds recently described bind in an allosteric pocket.³ⁿ Our X-ray crystal structure of TCU **2** bound to CHK1 shows that compound **2** is rotated by approximately 135° relative to compound **1** around an axis perpendicular to the thiophene ring (Figure 2b and Figure 2c). In this alternative binding mode, only two atoms of the inhibitor, the external NH of the urea and the carbonyl of the urea, form hydrogen bonds to the hinge region, while the aryl group now points toward the solvent channel. The protein–inhibitor contacts for deposited structures are summarized in Table 1. The TCU binding mode exemplified in the JNK1–**1** complex structure is not compatible with the DFG-in conformation observed in the CHK1–**2** complex. Asp169 from the DFG motif adopts a different conformation in the JNK1 structure compared with the corresponding Asp148 in CHK1. The conformation of the CHK1 aspartate (D148) would result in a steric clash with the aryl group were **2** to adopt the same binding mode as seen for **1** in JNK1 (Figure 2c). The structures of **1** and **2** bound to JNK1 and CHK1

suggested that while substitution of the amide would not be tolerated in JNK1, CDK1, or IKK β because of the structural differences, it would be in CHK1, thus opening a key avenue

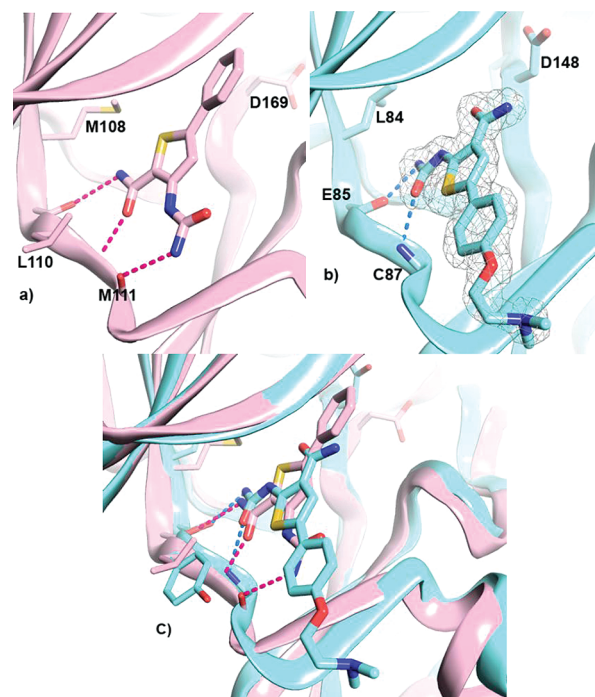


Figure 2. X-ray crystal structures of JNK1 and CHK1 in complex with selected compounds. The structures are oriented with the N-terminal lobe toward the top left, the C-terminal lobe toward the bottom right, and the hinge region on the bottom left. (a) X-ray crystal structure of **1** bound to JNK1 (PDB accession code 3PVE). Protein backbone cartoon and carbon atoms of the inhibitor are colored pink. Hydrogen bonds are indicated in magenta. (b) X-ray crystal structure of **2** bound to CHK1 (PDB accession code 2YDI). Protein backbone and carbon atoms of the inhibitor are colored pale blue. Hydrogen bonds are indicated in magenta. Final electron density ($2F_o - F_c$) contoured at 1.0σ is shown as a wire mesh. (c) Superposition of X-ray crystal structures of **1** with JNK1 and **2** with CHK1. The TCU binding mode differs between the two structures with the hinge binding donor–acceptor changing from the amide in the JNK1 structure to the urea in the CHK1 structure.

Table 1. Polar contacts between inhibitor and protein for deposited structures

compd	protein residue/atom	inhibitor functional group	inhibitor atom	distance (Å)	location	protein
1	E109/O	amide	N1	3.13	hinge	JNK1
1	M111/N	amide	O2	2.68	hinge	JNK1
1	M111/O	urea	N18	3.13	hinge	JNK1
2	E85/O	urea	N3	2.9	hinge	CHK1
2	C87/N	urea	O2	2.84	hinge	CHK1
3b	E85/O	urea	N2	2.77	hinge	CHK1
3b	C87/N	urea	O1	2.84	hinge	CHK1
3b	D148/OD2	piperidine	N4	2.73	ribose pocket	CHK1
3b	E134/O	piperidine	N4	2.83	ribose pocket	CHK1
3b	N135/OD1	piperidine	N4	2.94	ribose pocket	CHK1
4	E85/O	urea	N4	2.95	hinge	CHK1
4	C87/N	urea	O2	2.78	hinge	CHK1
4	D148/OD2	piperidine	N2	2.78	ribose pocket	CHK1
4	E134/O	piperidine	N2	2.82	ribose pocket	CHK1
4	E135/OD1	piperidine	N2	2.97	ribose pocket	CHK1

for inhibitor design with the aim of optimizing interactions with CHK1 as previously described.^{3b,5}

We recently reported on the structure-guided hit to lead identification, synthesis, and initial SAR of TCUs as CHK1 inhibitors,^{3b} work that led to the discovery of lead inhibitor **3b**. A library of compounds bearing both derivatized amides and *S*-aryl substitutions was designed and synthesized to explore potential interactions with residues in the CHK1 P-loop or in the vicinity of the ribose binding pocket.^{3b,10} From this initial SAR campaign and testing of a diverse set of compounds, it was evident that cyclic amine substitutions, such as homopiperidine or piperidine amide, yielded the most potent compounds as exemplified by **3a** and **3b** (Figure 1). Additionally, we determined that there was a strong stereochemical preference for the *S*-isomer, suggesting that **3a** and **3b** make specific interaction(s) in the CHK1 ATP-binding site in or in the vicinity of the ribose sugar pocket as predicted.

X-ray Crystal Structure of Lead **3b Bound to CHK1.** We obtained an X-ray crystal structure of **3b** bound to CHK1 (Figure 3) which provided an explanation for the preference of

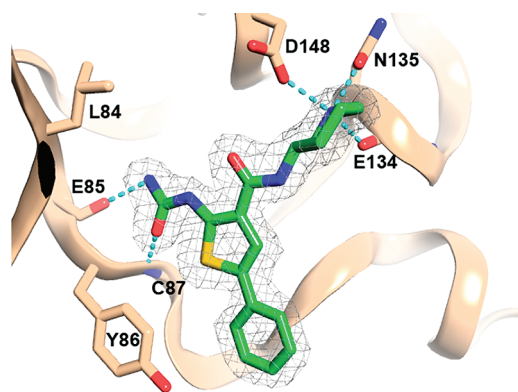


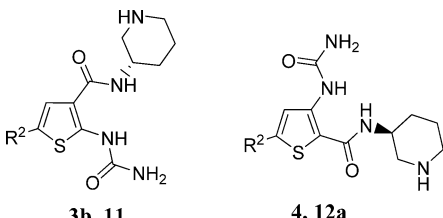
Figure 3. X-ray crystal structure of lead TCU Inhibitor **3b** in complex with CHK1 kinase (PDB accession code 2YDJ). The protein is oriented with the N-terminal lobe toward the top left, the C-terminal lobe toward the bottom right, and the hinge region on the bottom left. Protein backbone cartoon and carbon atoms of the protein are colored wheat, while carbon atoms of the inhibitor are colored green. Hydrogen bonds and salt bridges are shown as dotted blue lines. Final electron density ($2F_o - F_c$) contoured at 1σ is shown as a wire mesh. The polar contacts are summarized in Table 1.

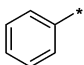
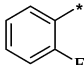
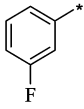
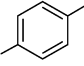
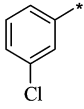
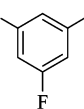
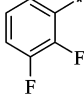
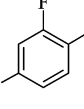
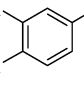
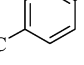
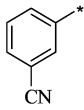
CHK1 for cyclic amines and the importance of correct chirality of the *3S*-aminopiperidine moiety. In addition to the two hydrogen bonding interactions with the hinge region of the adenine binding site, the protonated piperidine nitrogen of **3b** makes three polar interactions at the edge of the ribose binding pocket (Figure 3). These include a charge–charge or salt-bridge interaction with the carboxylate moiety of Asp-148, and charge–dipole interactions with the backbone carbonyl of Glu-134 and amide side chain of Asn-135 (see Table 1 for distance information). The backbone carbonyl interaction offers tetrahedral hydrogen bonding geometry (hydrogen atoms are not revealed by X-ray crystallography at this resolution). These three interactions, the charge–charge interaction and two charge–dipole interactions, explain why basic groups are preferred at this position. The preference for the *S*-enantiomer (**3b**) is presumably due to better positioning of the charged piperidine nitrogen to make these polar interactions. The *R*-enantiomer of **3b** (not shown) showed a 24-fold drop in potency ($IC_{50} = 0.17 \mu\text{M}$ compared to $0.008 \mu\text{M}$, Table 2). Targeting the ribose binding pocket not only allowed us to generate analogues with improved potency at the enzyme and cellular level against CHK1 but also afforded selectivity against CDK1 as predicted from the initial X-ray crystal structure of **2** in complex with CHK1^{3b} and based on the difference in the binding modes of the TCU scaffold seen in CHK1 and JNK1.

Thus, utilizing this structure-based design approach, we were able to generate high quality initial leads such as **3a** and **3b** bearing substituted amides from starting hit **2** and were subsequently poised to undergo an optimization campaign for delivering a preclinical candidate CHK1 inhibitor for cancer treatment in combination with DNA-damaging agents. Generation of the X-ray structure of **3b** bound to CHK1 validated our hypothesis for amide substitution resulting in key interactions surrounding the ribose binding pocket.

Optimization of the TCU Series of CHK1 Inhibitors.

We have previously reported the synthesis of **3a** and **3b**.^{3b,7} Several approaches to the lead optimization of **3b** were implemented. These included the generation of substituted ureas in an attempt to derive additional interactions with the Leu-84 gatekeeper residue to gain further selectivity for CHK1. Analogues of **3b** containing a variety of alkyl and aryl substitution on the urea were synthesized, allowing us to quickly determine this to be an unproductive avenue, as compounds were much less potent and solubility was not

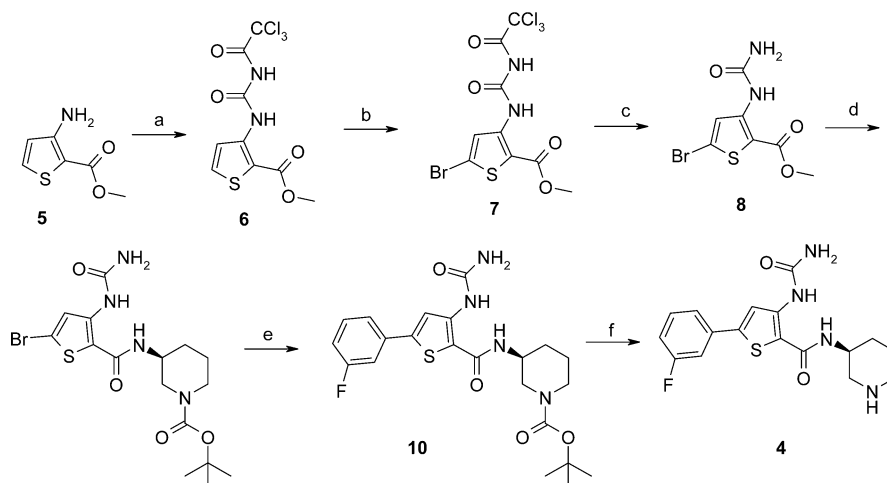
Table 2. SAR of 2-TCU and 3-TCU CHK1 Inhibitor Libraries^a


Compound	R ²	CHK1 IC ₅₀ (μM)	EC ₅₀ -CPT (μM)	EC ₅₀ -Alone (μM)
3b, 12a		0.007, 0.01	0.02, 0.02	0.45, 0.59
11a, 12b		0.009, 0.02	0.08, 0.02	1.06, 2.2
11b, 4		0.011, 0.005	0.02, 0.01	0.84, 0.28
11c, 12c		0.009, 0.006	0.03, 0.02	0.6, 13
11d, 12d		0.014, 0.008	0.04, 0.01	1.2, 0.7
11e, 12e		0.012, 0.01	0.03, 0.06	1.5, 2.5
11f, 12f		0.011, 0.02	0.1, 0.06	1.8, 1.5
11g, 12g		0.013, 0.03	0.19, 0.02	1.4, 1.1
11h, 12h		0.03, 0.04	0.15, 0.2	5.7, 5.8
11i, 12i		0.006, 0.006	0.008, 0.03	1.7, 0.6
11j, 12j		0.009, 0.007	0.94, 0.04	>13, 1.9

^aDepicted is a comparison of selected 3-TCUs with their 2-TCU matched pairs. 2-TCUs were generated as previously described.^{3b} 3-TCUs were synthesized using the method described for 4 in Scheme 1. EC₅₀-CPT represents cellular activity in cells pretreated with a DNA damaging agent, camptothecin, prior to compound treatment. EC₅₀-Alone represents cellular activity without any pretreatment. IC₅₀ represents activity of the compound in a CHK1 biochemical assay.

consistent with iv administration (data not shown). In another strategy, we pursued modification of the thiophene scaffold including ring replacement with a phenyl and a variety of

heterocyclic rings. A matched pair analysis comparing analogues of 3b containing a thiophene ring with those containing heterocycles or a phenyl ring indicated that the thiophene core

Scheme 1. Synthesis of 4^a

^aReagents and conditions: (a) TCA-N=C=O, THF, 90%; (b) bromine, acetic acid, reflux, 97%; (c) NH₃-MeOH (2 M), 99%; (d) *tert*-butyl (3*S*)-3-aminopiperidine-1-carboxylate, AlMe₃, THF, 40%; (e) 4-fluorophenylboronic acid, Pd(Ph₃P)₄, Cs₂CO₃, 1,4-dioxane/H₂O, 88%; (f) HCl/1,4-dioxane (4 M), rt, 4 h 84%.

was optimal for maintaining enzyme and cellular potency against CHK1 (data not shown). As a result of this campaign, however, we did identify a thiophene isomer with equivalent potency against CHK1.

Discovery of 3-Thiophenecarboxamide Urea (3-TCU) Inhibitors. Compound 3b contains a carboxamide at the 3-position and a urea at the 2-position of the thiophene, and thus, we refer to this scaffold as a 2-TCU. We envisioned that the regioisomer analogous to JNK1 inhibitor 1 having the urea in the 3-position and the amide in the 2-position could potentially bind to CHK1 in a similar fashion as the 2-TCUs, offering an additional opportunity for optimization.

In order to test this hypothesis, the matched pair 3-TCU 12a was synthesized using the method depicted in Scheme 1 for our clinical candidate 4. Reaction of commercially available methyl 3-aminothiophene-2-carboxylate (5) with trichloroacetyl isocyanate resulted in 6, which was brominated in acetic acid to give 7. Interestingly, while these bromination conditions proceeded at room temperature in the case of the positional isomer used to generate 3b,^{3b} bromination of 6 required heating to effect its transformation to 7. Deprotection of the urea with ammonia in methanol led to the formation of the corresponding thiophene ester 8. Weinreb amidation conditions similar to those previously reported for the 2-TCU series^{3b} were applied to 8 using *tert*-butyl (3*S*)-3-aminopiperidine-1-carboxylate to generate thiophene amide 9. Reaction of 9 with 3-fluorophenylboronic acid under Suzuki cross-coupling conditions resulted in arylthiophene 10. Final deprotection of the Boc group yielded the desired 3-TCU 12a as the hydrochloride salt. Using the same synthetic sequence, we generated a select number of analogues to derive SAR relative to the 2-TCU series. As shown in Figure 4, a head to head comparison of 2-TCU 3b (IC₅₀ = 7 nM) and matched pair 3-TCU 12a (IC₅₀ = 12 nM) reveals the compounds to be equivalent in their *in vitro* potency in both the biochemical CHK1 kinase assay and the HT29 cell abrogation assay described previously,^{3b,6} as expected by our prediction of similar binding modes. However, the 3-TCU series exemplified by 12a offer the added benefit of a 4-fold higher free compound

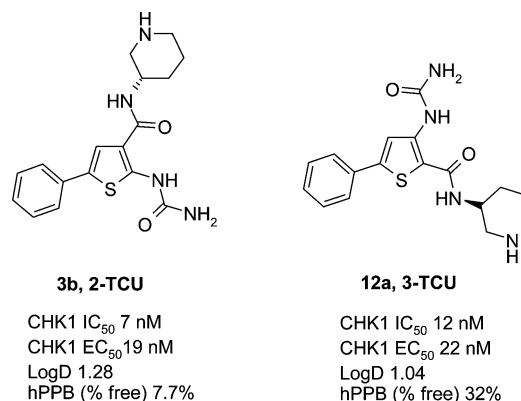


Figure 4. Comparison of lead 2-TCU and 3-TCU matched pairs.

fraction in the human plasma protein binding assay, a general trend observed across a broad range of the 3-TCUs.

Identification of Clinical Candidate 4 from Optimization of 3-TCU 12a. The CHK1–3b crystal structure shows that the phenyl ring on the 5-thienyl position projects into the CHK1 solvent channel. This position is therefore predicted to be tolerant of many substituents and functionality, allowing modulation of physicochemical and pharmacokinetic properties. As a final lead optimization strategy for the 3-TCU lead 12a, we thus carried out a multifactorial compound library campaign mainly focused on this position. This library was designed with the intent of increasing selectivity for CHK1 over other kinases while at the same time increasing oral bioavailability and improving pharmacokinetics and efficacy in the hollow fiber PD model and mouse animal models. Guided by X-ray structural information, we installed a diverse array of desired substituted aryl rings on the thiophene 5-position which were tolerable to CHK1 binding.

To that end, the key bromothiophene intermediate 9 shown in Scheme 1 was generated by Weinreb amidation^{8,9} and allowed us to quickly generate a large library of 5-position analogues using the Suzuki cross-coupling reaction as the means to introduce diversity. A subset of commercially available boronic acid and boronate esters were chosen to ensure

diversity in the final compound set and consisted of representative heterocyclic and aryl derivatives. Approximately 100 compounds were prioritized for synthesis and biological evaluation. The data for selected matched pairs are summarized in Table 2.

The X-ray crystal structure of **4** bound to CHK1, shown in Figure 5, confirmed the predicted binding mode. The urea at

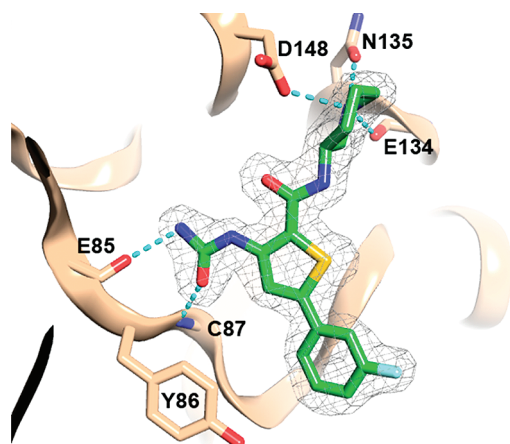


Figure 5. X-ray crystal structure of **4** in complex with CHK1 kinase (PDB accession code 2YDK) reveals that the binding mode of **3b** was preserved as predicted. The orientation is as in Figure 3. Protein backbone cartoon and carbon atoms are colored wheat, while carbon atoms of the inhibitor are colored green. Hydrogen bonds and salt bridges are shown as dotted blue lines. Final electron density ($2F_o - F_c$) contoured at 1σ is shown as a wire mesh. The polar contacts are as summarized in Table 1. The figure was generated using PYMOL.²²

the thiophene 3-position makes identical interactions to the hinge region as in the 2-TCU **3b**, albeit with the thiophene sulfur atom directed away from the hinge, and the 3-fluorophenyl substituent at the 5-position is directed toward the solvent channel.

Analogues **12a–j** and **4** were found to be very potent against CHK1 in vitro. The potencies of the 3-TCU series (**12a–j** and **4**) and their corresponding 2-TCU matched pairs^{10a} (**11a–j** and **3b**) were generally almost identical. Determination of the 3-TCU series SAR was derived from a Topliss-like^{10b} examination of size, functionality, and electronic variation through comprehensive substitutions on the phenyl ring of **12a**. For example, when the ortho, meta, and para fluorine substitutions were compared (Table 2), it was evident that substitution at the ortho position (**12b**) was less favorable with regard to kinase activity but meta (**4**) and para (**12c**) analogues had improved CHK1 activity and similar potency. Size had minimal effect on activity, as demonstrated by the finding that chloro, cyano, and other electron withdrawing functional groups did not result in any significant change in activity, but we did find much variation on cellular potency. Electron donating groups such as dimethylamino and methoxy tended to be slightly less potent and followed similar trends as reported for the 2-TCU series.^{3b} Examination of heterocyclic replacements of the aryl group resulted in compounds that maintained potency in both the enzyme and cellular assays, similar to that reported earlier in the 2-TCU series^{3b} (data not shown).

All compounds were tested both alone and in combination with camptothecin in the HT29 cellular checkpoint abrogation assay^{3a} to determine the extent of abrogation directly related to CHK1 inhibition versus off-target cellular activities. While some

compounds show activity in the absence of DNA damage, in most cases there is a >100-fold increase in potency in the pretreated group for both the 2-TCU and 3-TCU series. A number of potent compounds were identified in our in vitro assays, paying special attention to physical properties like solubility in addition to protein binding consistent with the iv route of administration. Thermodynamic solubility data were generated at pH 7.4 (0.1 M phosphate buffer). These compounds were further differentiated by means of our in vivo cascade that includes pharmacodynamic (PD) activity and efficacy. Nude mouse pharmacokinetic (PK) profiles for selected matched pairs are summarized in Table 3.

Table 3. Mouse PK (Nude) of Selected Matched Pairs

2-TCU

3-TCU

TCU	nude mouse	R = 4-F		
		11c, 12c	11b, 4	11f, 12f
2-TCU: 11c, 11b, 11f	AUC ($\mu\text{M}\cdot\text{h}$)	1.5	3.8	1.7
	Cl ($\text{mL min}^{-1} \text{kg}^{-1}$)	81	33	71
	$T_{1/2}$ (h)	1.2	1	1.2
	V_{ss} (l/kg)	6.1	2.8	4.5
3-TCU: 12c, 4, 12f	AUC ($\mu\text{M}\cdot\text{h}$)	1.46	2.5	1.4
	Cl ($\text{mL min}^{-1} \text{kg}^{-1}$)	86	50	85
	$T_{1/2}$ (h)	1.2	1.1	1.4
	V_{ss} (l/kg)	8.5	3.9	7.7

A comparison of PK parameters for 2-TCUs (**11c, 11b**, and **11f**) and their 3-TCU matched pairs (**12c, 4, 12f**) demonstrates that while they are equivalent in their PK properties, 3-F substituted positional isomers **11b** and **4** consistently show lower clearance. 3-TCU **4** could be further differentiated from **11b** by its higher solubility (>1 mM compared to 779 μM) and lower plasma protein binding (hPPB, see Figure 7B), an important consideration given the planned iv route of administration. Several 2- and 3-TCUs were screened in a high throughput pharmacodynamic (PD) assay which aided the prioritization of compounds for efficacy studies (see below). These data, along with the overall safety and selectivity profile, enabled the selection of **4** as the clinical candidate.⁶

Evaluation of 4 in the Hollow Fiber PD Assay. The hollow fiber PD assay, described in detail in an earlier publication,^{6a} was used to determine the in vivo PD activity of selected CHK1 inhibitors to assist prioritization of compounds for testing in xenograft efficacy models. Briefly, cells were treated with the DNA-damaging agent topotecan to induce cell cycle arrest in the G2 phase. Following cell cycle arrest, the hollow fibers are filled with cells and implanted under the skin of the animal. This arrest is stable for up to 30 h after implantation in the absence of treatment with a CHK1 inhibitor. Compounds are then administered at 10 mg/kg using iv dosing. Finally, fibers are retrieved after 30 h, and the cell

cycle profile is determined with propidium iodide staining using flow cytometry. In animals dosed with CHK1 inhibitors, the G2 checkpoint is overcome causing a reduction in the number of cells in G2 and a concomitant increase in the number of cells re-entering the G1 phase. The “odds value” is then calculated as the ratio of the G2/G1 populations for topotecan alone and the CHK1 inhibitor combination. From the latter, we calculated an odds ratio (OR) that allowed quantitative assessment of the degree of checkpoint abrogation. The greater the OR, the higher is the level of checkpoint abrogation. Shown in Table 4

Table 4. PD Activity of Selected 2-TCUs and 3-TCUs

2-TCU	OR ^a at 10 mg/kg (iv)	control ^b	3-TCU	OR ^a at 10 mg/kg (iv)	control ^b
3b ^c	4.56	0.00	12a	3.12	<0.05
11a	2.14	0.013	12b	2.04	0.024
11b ^d	2.89	0.001	4	5.01	0.000
11d	1.91	0.37	12d	4.61	0.000
11g	1.59	0.138	12g	2.96	0.001
11i	2.62	0.002	12i	3.79	<0.05

^aOR = odds ratio. ^bControl = compound alone run in the absence of a DNA damaging agent. ^cAverage of eight runs. ^dAverage of two runs.

are the OR values for selected 2- and 3-TCUs demonstrating the superiority of **4** over others in the series based on its high OR value and lack of activity in the control arm of the experiment (which reflects the extent of CHK1 selectivity shown by the inhibitor).

Treatment with compound **4** resulted in the abrogation of the G2 checkpoint in a dose dependent manner, as shown in Figure 6.^{6a} In general, our data show a good correlation

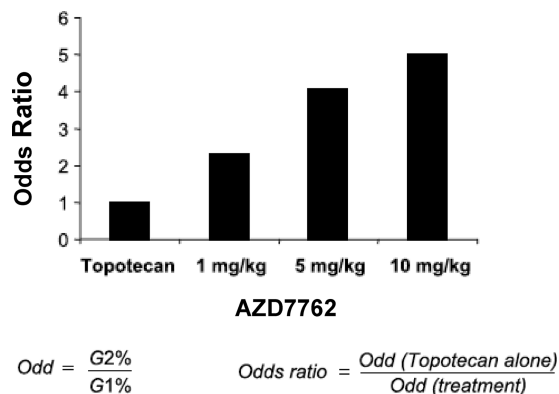


Figure 6. Dose dependent increase in the odds ratio (OR) observed with AZD7762 (iv administration).

between the relative potency of inhibitors as measured in the cellular checkpoint abrogation assay and the observed PD effect. An exposure of 8 h above EC₅₀ was required in order to obtain maximal PD activity.^{6a} There were also many examples of compounds showing potency in vitro and yet lacking in vivo activity in the PD model. We were able to explain this discrepancy in the majority of cases through differences in PK profiles among analogues.

Antitumor Efficacy Potentiation of DNA Damaging Chemotherapeutics by **4.**^{6a} The ability of **4** to potentiate the efficacy of both gemcitabine and irinotecan was evaluated in mouse and rat xenograft models and is described in detail in an earlier publication.^{6a} In each case, strong potentiation of the

efficacy of DNA damage inducing chemotherapeutics by **4** was observed.

Kinase Selectivity Profile of Preclinical Candidate **4.** The kinase selectivity of **4** was checked by profiling against a large panel of diverse Ser/Thr and Tyr protein kinases from Upstate/Millipore in which examples of each kinase class are represented. Key data for the screen are summarized in Figure 7C. In general, kinases showing less than 10-fold selectivity were from the same kinase family (CAMK) as CHK1 or were Src-family tyrosine kinases (Yes, Fyn, Lyn, Hck, and Lck but not Src itself). Following preliminary profiling, expanded screening was biased toward CAMK and tyrosine kinase family members. Data generated from in-house and external screening in the Upstate/Millipore kinase panel indicated good selectivity (>10-fold) for CHK1 kinase versus 164 kinases. Importantly, selectivity was shown in the cyclin-dependent kinase 1 (CDK1)/cyclin B1 scintillation proximity assay (>1000-fold) and against other CDKs tested. A greater than 100-fold selectivity against multiple protein kinase C isoforms, CDKs, p38 (all isoforms), and MAPKAPK2 clearly differentiated the activity profile of **4** from UCN-01, a known inhibitor of CHK1. Compound **4** is an equally potent inhibitor of CHK1 and CHK2 in vitro; hence, the phenotypic response cannot be presumed to be arising from CHK1 inhibition alone based on data from the experiments presented herein. Literature precedent, however, has indicated a major role for CHK1 versus CHK2 when both kinases were assessed simultaneously.^{11,12}

On the basis of the comparison of the key data presented in Figure 7 against other compounds in the 2-TCU and 3-TCU series combined with its efficacy and tolerability profile, compound **4** was selected as a clinical candidate and entered phase I in combination with gemcitabine or irinotecan.

CONCLUSION

TCUs were identified as potent ATP-competitive CHK1 inhibitors in an HTS campaign of the AstraZeneca compound collection followed by expedient hit to lead identification and optimization employing protein–ligand crystal structures to rationally guide compound design and optimization. TCUs are known inhibitors of IKK2 and JNK1 kinases. The X-ray crystal structure of the original HTS hit **2** in complex with CHK1 highlighted substitution at the amide moiety as a means to achieve productive interactions with key residues in the ribose binding pocket, thereby increasing the potency. Substitution on the amide was additionally advantageous in affording selectivity over CDKs, IKKβ, and JNK1, where by virtue of an alternative binding mode, substitution at the amide is not tolerated. Optimization of the 2-TCU by pursuing amide libraries led to the identification of the 3-(S)-piperidinylamide analogue **3b**. The crystal structure of CHK1 in complex with **3b** revealed key polar interactions in the ribose pocket, which account for the increase in potency and enantiomeric preference at this position. Exploration of alternative scaffolds led us to focus on a positional isomer of **3b**, which resulted in the rational design of lead 3-TCU **12a** and corresponding 3-TCU subseries, which we found to be of equivalent potency compared to the 2-TCUs with the added benefit of an improved DMPK profile and in vivo efficacy. A Suzuki library of 5-substituted 3-TCUs, designed to target the CHK1 solvent channel and thus modulate PK and physicochemical properties, resulted in the discovery of a large number of tolerated substitutions and identified a 3-fluorophenyl moiety as an optimal analogue of

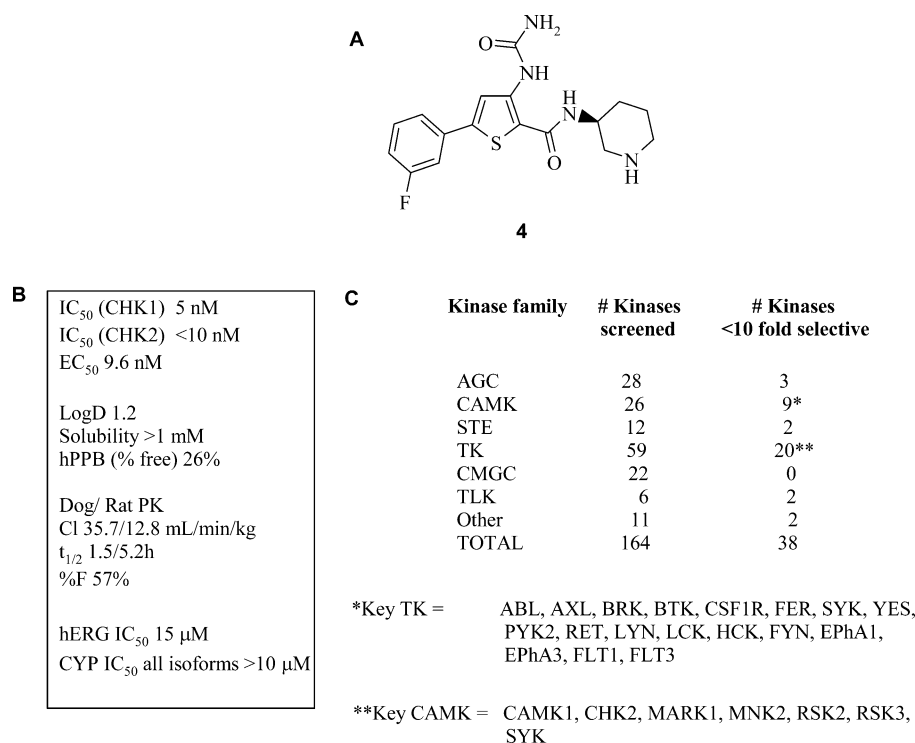


Figure 7. (A) Structure of AZD7762. (B) In vitro and in vivo profile. (C) Kinase family selectivity profile.

the 5-phenyl group. Hybridization of these key structural features led to the identification of the development candidate **4** with suitable in vitro, in vivo, and safety profiles. An additional key feature of **4** is >1 mM solubility, an important consideration given the clinical route of administration is intravenous. The development candidate **4** and the related TCU class of CHK1 inhibitors strongly potentiate the effects of DNA damage caused by cytotoxic agents such as gemcitabine or irinotecan as well as when combined with radiation therapy in a variety of preclinical models.^{6d,13} Clinical trials of **4** were terminated after a full review of program data. Termination of the study was made after a full review of program data and assessment of the current risk–benefit profile. Both CHK1 and CHK2 checkpoint kinase inhibitors remain an active area of research and clinical development.

EXPERIMENTAL SECTION

General. All solvents used are anhydrous and commercially available. All commercially available materials were used without further purification unless otherwise stated. ¹H NMR spectra were recorded on Bruker 300 or 400 MHz NMR spectrometers. Chemical shifts are expressed in parts per million (ppm, δ) relative to tetramethylsilane (TMS) as an internal standard using deuterated chloroform as a solvent unless otherwise indicated. All NMR chemical shifts are reported as δ values in parts per million (ppm). The splitting pattern abbreviations are as follows: s, singlet; d, doublet; t, triplet; q, quartet; br, broad; br s, broad singlet; m, unresolved multiplet due to the field strength of the instrument; dd, doublet of doublet; dt, doublet of triplet; ddd, doublet of doublet of doublet. Analytical mass spectra were run with an electron energy of 70 eV in the chemical ionization (CI) mode using a direct exposure probe, where the indicated ionization was effected by electron impact (EI), electrospray (ESP), or atmospheric pressure chemical ionization (APCI). Values for M + H are given; generally, only ions that indicate the parent mass are reported. The purity of all final compounds was confirmed by analysis with an Agilent 1100 liquid chromatography unit (LC) with an Agilent 1100 mass spectrometry detector (MSD) or a Waters ZQ mass

spectrometer (compounds were detected by mass spectrometry in APCI+ ionization) using a Luna 3 μm C8 (2) column (100A, 30–2.0 mm), eluting with mixtures of water–acetonitrile (ranging from 5% to 98% acetonitrile/water with 0.1% formic acid), using a UV detector at 220, 240, and 254 nm. The purity of all final compounds was at least 95%. Reverse phase chromatography was performed with Gilson systems using a YMC-AQC18 reverse phase HPLC column with dimensions 20 mm/100 and 50 mm/250 in water/MeCN with 0.1% TFA as mobile phase. Silica gel chromatography was performed using either glass column packed with silica gel (200–400 mesh, Aldrich Chemical) or prepacked silica gel cartridges (Biotage and ISCO CombiFlash systems)

Methyl 3-(((Trichloroacetyl)amino)carbonyl)amino)thiophene-2-carboxylate (6). To a stirred solution of methyl 3-aminothiophene-2-carboxylate (17.0 g, 108 mmol) in anhydrous THF (216 mL) was added trichloroacetyl isocyanate (12.9 mL, 108 mmol) slowly over a period of 20 min. After the addition was complete, a precipitate formed and the mixture stirred for an additional 1 h at room temperature. The desired product was obtained by filtration to give **6** (36.8 g, 99%) as an off-white solid and was used without further purification for synthesis of **7**. LC/MS (APCI, ES): (M + H)⁺ 345.

Methyl 5-Bromo-3-(((trichloroacetyl)amino)carbonyl)amino)thiophene-2-carboxylate (7). To a solution of **6** (10.11 g, 29.38 mmol) in glacial acetic acid (146 mL) at 0 °C was added slowly a solution of bromine (46.4 mL, 90 mmol) in glacial acetic acid (38 mL). The resulting cloudy solution was heated to 70 °C for 3 h when the mixture was cooled to room temperature. The desired product was collected by filtration and the filtrate was washed with ether and dried under vacuum to obtain the desired product as a white solid (12 g, 97%), which was used for preparation of **8** without further purification. LC/MS (APCI, ES): (M + H)⁺ 424.

Methyl 3-((Aminocarbonyl)amino)-5-bromothiophene-2-carboxylate (8). A solution of **7** (12 g, 28.3 mmol) in dry MeOH (60 mL) was purged with gaseous NH₃ at 0 °C until the solution became clear. The mixture was stirred for 20 min at room temperature, and evaporation gave the desired product (7.8 g, 99%) as white solid. ¹H NMR (DMSO-*d*₆): δ 9.35 (s, 1H), 8.10 (s, 1H), 6.90 (br s, 2H), 3.82 (s, 3 H). LC/MS (APCI, ES): (M + H)⁺ 280.

tert-Butyl (3S)-3-[[[3-[(Aminocarbonyl)amino]-5-bromo-2-thienyl]carbonyl]amino]piperidine-1-carboxylate (9). To a solution of **8** (1.6 g, 5.7 mmol) in dry THF (30 mL) was added a solution of $\text{Me}_3\text{Al}/\text{tert-butyl (3S)-3-aminopiperidine-1-carboxylate}$ in THF (18 mL) (performed by the addition of Me_3Al (17.2 mL, 34.4 mmol) to a solution of *tert-butyl (3S)-3-aminopiperidine-1-carboxylate* (3.7 g, 17.2 mmol) in THF at -78°C , and the resulting yellow solution was stirred at this temperature for 15 min), and the resulting deep yellow solution was warmed to room temperature and stirred overnight. The reaction mixture was cooled with ice, and a saturated solution of sodium potassium tartrate was added to quench the reaction. The mixture was partitioned between EtOAc and H_2O (3:1 ratio). The aqueous layer was extracted with EtOAc (3 \times), and the combined organic extracts were washed with H_2O , brine and dried over MgSO_4 . Evaporation gave a pale orange solid. Purification by reverse phase HPLC using a gradient of 5–95% MeCN in 0.1% TFA containing water gave the desired product as an off-white solid (1.0 g, 40%). $^1\text{H NMR}$ ($\text{DMSO}-d_6$): δ 10.06 (s, 1H), 8.02 (s, 1H), 7.89 (d, 1H), 6.71 (br s, 2H), 4.04 (m, 1H), 3.72 (m, 2H), 2.74 (m, 2H), 1.81 (m, 1H), 1.68 (m, 1H), 1.52 (m, 1H), 1.37 (s, 9H), 1.34 (m, 1H). LC/MS (APCI, ES): (M + H) $^+$ 448.

tert-Butyl (3S)-3-[[[3-[(Aminocarbonyl)amino]-5-(3-fluorophenyl)-2-thienyl]carbonyl]amino]piperidine-1-carboxylate (10). In a round bottomed flask, **9** (1 g, 2.24 mmol), 3-fluorobenzenboronic acid (0.5 g, 3.36 mmol), and cesium carbonate (2.9 g, 8.96 mmol) were dissolved in a mixture of water (3 mL) and 1,4-dioxane (20 mL). The solution was degassed under low vacuum and nitrogen. Palladium(0) tetrakis(triphenylphosphine) was added (0.26 g, 0.22 mmol) to the solution, and the colorless reaction mixture was heated at 75°C with stirring for 1 h. The aqueous layer was separated. Ethyl acetate was added (20 mL), and the resulting solution was dried over MgSO_4 (anhydrous). After solvent evaporation the residual solid was subjected to flash chromatography on silica gel (40 g) with 2–5% methanol in DCM over a 30 min gradient. The main fraction contained traces of triphenylphosphine oxide and was resubjected to flash chromatography under the same conditions to afford a light yellow solid (0.92 mg, 88%). $^1\text{H NMR}$ (CDCl_3): δ 10.35 (s, 1H), 8.30 (s, 1H), 7.43–7.28 (m, 3H), 7.05 (m, 1H), 5.91 (br s, 1H), 4.79 (br s, 2H), 4.05 (m, 1H), 3.53–3.55 (m, 2H), 3.36–3.29 (m, 2H), 1.89–1.49 (m, 13H). LC/MS (APCI, ES): (M + H) $^+$ 463.

5-(2-Fluorophenyl)-2-ureidothiophene-3-carboxylic Acid (S)-Piperidin-3-ylamide Hydrochloride (4). Intermediate **10** (0.92 g, 1.98 mmol) was dissolved in methanol (7 mL), and 4 M HCl in dioxane (10 mL, 40 mmol) was added while cooling at 0°C . The solution was stirred for 3 h. The solvent was evaporated under reduced pressure, and the residue was taken in methanol (20 mL) and evaporated to dryness. This procedure was repeated 5 times to yield a white powder. The solid was dissolved in water (10 mL) and filtered, and solvent was evaporated by lyophilization over 48 h to obtain a light yellow solid (0.67 g, 84%). $^1\text{H NMR}$ ($\text{DMSO}-d_6$): δ 10.98 (s, 1H), 9.29 (s, 1H), 9.20 (s, 1H), 8.43 (d, 1H), 8.06 (s, 1H), 7.77 (m, 2H), 7.29 (m, 3H), 7.08 (br, 2H), 4.25 (s, 1H), 3.29 (d, 1H), 3.14 (d, 1H), 2.92 (m, 2H), 1.93 (d, 2H), 1.67 (m, 2H). LC/MS (APCI, ES): (M + H) $^+$ 363.

Application of this two-step procedure described above for synthesizing **4** from **10** enabled generation of compounds **11a–j** and **12a–j** as hydrochloride salts.

5-(2-Fluorophenyl)-2-ureidothiophene-3-carboxylic Acid (S)-Piperidin-3-ylamide (11a). $^1\text{H NMR}$ ($\text{DMSO}-d_6$): δ 10.98 (s, 1H), 9.29 (s, 1H), 9.20 (s, 1H), 8.43 (d, 1H), 8.06 (s, 1H), 7.77 (m, 2H), 7.29 (m, 3H), 7.08 (br, 2H), 4.25 (s, 1H), 3.29 (d, 1H), 3.14 (d, 1H), 2.92 (m, 2H), 1.93 (d, 2H), 1.67 (m, 2H). LC/MS (APCI, ES): (M + H) $^+$ 363.

5-(3-Fluorophenyl)-2-ureidothiophene-3-carboxylic Acid (S)-Piperidin-3-ylamide (11b). $^1\text{H NMR}$ ($\text{DMSO}-d_6$): δ 10.94 (s, 1H), 8.98 (d, 2H), 8.27 (d, 2H), 8.03 (s, 1H), 7.40 (m, 3H), 7.08 (t, 2H), 4.19 (s, 1H), 3.30 (m, 1H), 3.18 (d, 1H), 2.93 (m, 2H), 1.93 (d, 2H), 1.67 (m, 2H). LC/MS (APCI, ES): (M + H) $^+$ 363.

5-(4-Fluorophenyl)-2-ureidothiophene-3-carboxylic Acid (S)-Piperidin-3-ylamide (11c). $^1\text{H NMR}$ ($\text{DMSO}-d_6$): δ 1.68 (m,

2 H), 1.92 (d, 2 H), 2.92 (m, 2 H), 3.17 (d, 1 H), 3.30 (d, 1 H), 4.21 (s, 1 H), 7.03 (s, 2 H), 7.25 (t, 2 H), 7.59 (t, 2 H), 7.92 (s, 1 H), 8.31 (d, 1 H), 9.07 (d, 2 H), 10.90 (s, 1 H). LC/MS (APCI, ES): (M + H) $^+$ 363.

5-(3-Chlorophenyl)-2-ureidothiophene-3-carboxylic Acid (S)-Piperidin-3-ylamide (11d). $^1\text{H NMR}$ ($\text{DMSO}-d_6$): δ 10.94 (s, 1H), 9.10 (s, 1H), 8.30 (d, 1H), 8.06 (s, 1H), 7.61 (s, 1H), 7.49 (d, 1H), 7.42 (t, 1H), 7.30 (d, 1H), 7.09 (s, 2H), 4.21 (s, 1H), 3.32 (d, 1H), 3.17 (d, 1H), 2.92 (t, 2H), 1.93 (d, 2H), 1.68 (m, 2H). LC/MS (APCI, ES): (M + H) $^+$ 379.

5-(3,5-Difluorophenyl)-2-ureidothiophene-3-carboxylic Acid (S)-Piperidin-3-ylamide (11e). $^1\text{H NMR}$ ($\text{DMSO}-d_6$): δ 10.95 (s, 1H), 9.10 (s, 1H), 8.98 (s, 1H), 8.32 (d, 1H), 8.16 (s, 1H), 7.26 (d, 2H), 7.12 (t, 2H), 4.22 (s, 1H), 3.28 (d, 1H), 3.17 (d, 1H), 2.95 (m, 2H), 1.91 (d, 2H), 1.65 (m, 2H). LC/MS (APCI, ES): (M + H) $^+$ 381.

5-(2,3-Difluorophenyl)-2-ureidothiophene-3-carboxylic Acid (S)-Piperidin-3-ylamide (11f). $^1\text{H NMR}$ ($\text{DMSO}-d_6$): δ 11.01 (s, 1H), 9.22 (s, 1H), 9.14 (s, 1H), 8.46 (d, 1H), 8.10 (s, 1H), 7.81 (t, 1H), 7.29 (m, 2H), 7.11 (br, 2H), 4.20 (s, 1H), 3.30 (d, 1H), 3.14 (d, 1H), 2.92 (m, 2H), 1.90 (d, 2H), 1.69 (m, 2H). LC/MS (APCI, ES): (M + H) $^+$ 381.

5-(2,4-Difluorophenyl)-2-ureidothiophene-3-carboxylic Acid (S)-Piperidin-3-ylamide (11g). $^1\text{H NMR}$ ($\text{DMSO}-d_6$): δ 10.97 (s, 1H), 9.30 (s, 1H), 9.18 (s, 1H), 8.45 (d, 1H), 8.02 (s, 1H), 7.78 (q, 1H), 7.38 (t, 1H), 7.18 (t, 1H), 7.06 (br, 2H), 4.23 (s, 1H), 3.29 (d, 1H), 3.14 (d, 1H), 2.92 (m, 2H), 1.90 (d, 2H), 1.69 (m, 2H). LC/MS (APCI, ES): (M + H) $^+$ 381.

5-(3,4-Dichlorophenyl)-2-ureidothiophene-3-carboxylic Acid (S)-Piperidin-3-ylamide (11h). $^1\text{H NMR}$ ($\text{DMSO}-d_6$): δ 10.96 (s, 1H), 9.30 (s, 1H), 9.19 (s, 1H), 8.43 (d, 1H), 8.18 (s, 1H), 7.79 (s, 1H), 7.63 (d, 1H), 7.51 (d, 1H), 7.10 (br, 2H), 4.24 (s, 1H), 3.29 (d, 1H), 3.13 (d, 1H), 2.94 (m, 2H), 1.92 (d, 2H), 1.70 (m, 2H). LC/MS (APCI, ES): (M + H) $^+$ 413.

5-(4-Cyanophenyl)-2-ureidothiophene-3-carboxylic Acid (S)-Piperidin-3-ylamide (11i). $^1\text{H NMR}$ ($\text{DMSO}-d_6$): δ 10.98 (s, 1H), 9.03 (s, 2H), 8.37 (d, 1H), 8.22 (s, 1H), 7.84 (d, 2H), 7.72 (d, 2H), 7.14 (s, 2H), 4.20 (s, 1H), 3.31 (d, 1H), 3.17 (d, 1H), 2.93 (t, 2H), 1.93 (d, 2H), 1.67 (m, 2H). LC/MS (APCI, ES): (M + H) $^+$ 370.

5-(3-Cyanophenyl)-2-ureidothiophene-3-carboxylic Acid (S)-Piperidin-3-ylamide (11j). $^1\text{H NMR}$ ($\text{DMSO}-d_6$): δ 10.94 (s, 1H), 9.01 (s, 2H), 8.28 (d, 1H), 8.11 (s, 1H), 7.98 (s, 1H), 7.83 (d, 2H), 7.71 (d, 1H), 7.61 (t, 1H), 7.12 (s, 2H), 4.18 (s, 1H), 3.18 (d, 2H), 2.91 (m, 2H), 1.93 (d, 2H), 1.68 (m, 2H). LC/MS (APCI, ES): (M + H) $^+$ 370.

5-Phenyl-3-ureidothiophene-2-carboxylic Acid (S)-Piperidin-3-ylamide (12a). $^1\text{H NMR}$ ($\text{DMSO}-d_6$): δ 10.02 (s, 1H), 9.39 (brs, 2H), 8.25 (s, 1H), 8.18 (d, 1H), 7.6 (d, 2H), 7.58–7.31 (m, 3H), 4.19 (m, 1H), 3.34–3.12 (m, 2H), 2.83 (m, 2H), 1.90–1.51 (m, 4H). LC/MS (APCI, ES): (M + H) $^+$ 345.

5-(2-Fluorophenyl)-3-ureidothiophene-2-carboxylic Acid (S)-Piperidin-3-ylamide (12b). $^1\text{H NMR}$ ($\text{DMSO}-d_6$): δ 9.95 (s, 1H), 8.66 (s, 2H), 7.84–8.02 (m, 1H), 8.15 (d, 1H), 7.70–7.86 (m, 1H), 7.22–7.57 (m, 3H), 7.10 (s, 1H), 6.69 (s, 1H), 3.79–4.58 (m, 2H), 3.11–3.36 (m, 2H), 2.77–3.05 (m, 1H), 1.74–2.21 (m, 3H), 1.47–1.75 (m, 1H). LC/MS (APCI, ES): (M + H) $^+$ 363.

5-(4-Fluorophenyl)-3-ureidothiophene-2-carboxylic Acid (S)-Piperidin-3-ylamide (12c). $^1\text{H NMR}$ ($\text{DMSO}-d_6$): δ 9.94 (s, 1H), 8.73 (s, 2H), 8.22 (s, 1H), 8.08 (d, $J = 7.54$ Hz, 1H), 7.56–7.76 (m, 2H), 7.19–7.44 (m, 2H), 6.68 (s, 2H), 4.05–4.28 (m, 1H), 3.07–3.48 (m, 2H), 2.67–3.00 (m, 2H), 1.88 (s, 2H), 1.53–1.68 (m, 2H). LC/MS (APCI, ES): (M + H) $^+$ 363.

5-(3-Chlorophenyl)-3-ureidothiophene-2-carboxylic Acid (S)-Piperidin-3-ylamide (12d). $^1\text{H NMR}$ ($\text{DMSO}-d_6$): δ 9.85 (s, 1H), 8.58 (s, 2H), 8.30 (s, 1H), 8.07–8.14 (m, 1H), 8.05 (s, 1H), 7.88 (d, 1H), 7.81 (d, 1H), 7.62 (t, 1H), 6.65 (s, 1H), 3.92–4.29 (m, 1H), 3.08–3.28 (m, 2H), 2.70–2.87 (m, 2H), 1.72–1.91 (m, 2H), 1.44–1.71 (m, 2H). LC/MS (APCI, ES): (M + H) $^+$ 379.

5-(3,5-Difluorophenyl)-3-ureidothiophene-2-carboxylic Acid (S)-Piperidin-3-ylamide (12e). $^1\text{H NMR}$ ($\text{DMSO}-d_6$): δ 9.89 (s, 1H), 9.19 (br s, 2H), 8.32 (s, 1H), 8.30 (d, 1H), 7.28 (m, 3H), 6.62

(br s, 1H), 4.18 (m, 1H), 3.18 (m, 2H), 2.78 (m, 2H), 1.89–1.42 (m, 4H). LC/MS (APCI, ES): (M + H)⁺ 381.

5-(2,3-Difluorophenyl)-3-ureidothiophene-2-carboxylic Acid (S)-Piperidin-3-ylamide (12f). ¹H NMR (DMSO-*d*₆): δ 9.89 (s, 1H), 9.02 (br s, 2H), 8.35 (s, 1H), 8.20 (d, 1H), 7.68–7.20 (m, 3H), 6.68 (br s, 1H), 4.15 (m, 1H), 3.18 (m, 2H), 2.80 (m, 2H), 1.89–1.50 (m, 4H). LC/MS (M + H)⁺ 381.

5-(2,4-Difluorophenyl)-3-ureidothiophene-2-carboxylic Acid (S)-Piperidin-3-ylamide (12g). ¹H NMR (DMSO-*d*₆): δ 9.89 (s, 1H), 8.90 (br s, 2H), 8.32 (s, 1H), 8.17 (d, 1H), 7.78 (q, 1H), 7.48 (t, 1H), 7.22 (t, 1H), 6.68 (br s, 1H), 4.18 (m, 1H), 3.18 (m, 2H), 2.78 (m, 2H), 1.89–1.42 (m, 4H). LC/MS (APCI, ES): (M + H)⁺ 381.

5-(3,4-Dichlorophenyl)-3-ureidothiophene-2-carboxylic Acid (S)-Piperidin-3-ylamide (12h). ¹H NMR (DMSO-*d*₆): δ 9.82 (s, 1H), 9.12 (s, 1H), 8.98 (br s, 1H), 8.22 (s, 1H), 8.17 (d, 1H), 7.78 (s, 1H), 7.70 (d, 1H), 7.50 (s, 1H), 6.62 (br s, 1H), 4.18 (m, 1H), 3.18 (m, 2H), 2.78 (m, 2H), 1.89–1.42 (m, 4H). LC/MS (APCI, ES): (M + H)⁺ 414.

5-(4-Cyanophenyl)-3-ureidothiophene-2-carboxylic Acid (S)-Piperidin-3-ylamide (12i). ¹H NMR (DMSO-*d*₆): δ 9.82 (s, 1H), 8.98 (br s, 1H), 8.32 (s, 1H), 8.19 (d, 1H), 7.82 (d, 2H), 7.76 (d, 2H), 6.62 (br s, 1H), 4.18 (m, 1H), 3.18 (m, 2H), 2.78 (m, 2H), 1.89–1.42 (m, 4H). LC/MS (APCI, ES): (M + H)⁺ 370.

5-(3-Cyanophenyl)-3-ureidothiophene-2-carboxylic Acid (S)-Piperidin-3-ylamide (12j). ¹H NMR (DMSO-*d*₆): δ 9.86 (s, 1 H), 8.43–8.76 (m, 2 H), 8.06 (d, 2 H), 7.56–7.67 (m, 1 H), 7.40–7.47 (m, 2 H) 7.54 (s, 1 H), 6.64 (s, 1 H), 3.91–4.25 (m, 1 H), 3.20 (dd, 4 H), 2.62–2.88 (m, 2 H), 1.76–1.87 (m, 2 H), 1.43–1.66 (m, 2 H). LC/MS (APCI, ES): (M + H)⁺ 370.

CHK1 Kinase Assay.^{6a} Recombinant human CHK1 was expressed as a glutathione S-transferase fusion in insect cells using a baculovirus vector and purified by glutathione affinity chromatography. A synthetic peptide substrate for CHK1 was synthesized by Bachem (*N*-biotinylaminohexanoyl-KKVSRSGLYRSPMPENLNRRP). Compounds were screened at a single concentration (10 μmol/L) for the primary assay using a standard scintillation proximity assay protocol. For follow-up, a dose response was determined (IC₅₀). Final assay concentrations of peptide and ATP (cold + 40 nCi [³³P]ATP) were 0.8 and 1 μmol/L, respectively. In brief, compound and buffer containing peptide and kinase and ATP were added sequentially to a 384-well assay plate. The plate was incubated for 2 h. Reaction was stopped by the addition of buffer containing EDTA and scintillation proximity assay beads (Amersham), and plates were read using a TopCount reader (Packard). Data analysis was carried out using proprietary software.

For kinetic analysis, a filter binding assay was used. The assay reaction contained the reagents listed above but with the following concentrations of ATP [0–600 μmol/L (cold + Ci [³³P]ATP), determined *K*_m], Chk1 (0.5 nmol/L), and **4** (0, 1.5, 5, 10 nmol/L). The mixture was incubated at room temperature for 20 min. The reaction was stopped by the addition of EDTA. The mixture was transferred to streptavidin FlashPlate (Perkin-Elmer), incubated at room temperature for 1 h, and aspirated out, and wells were washed with PBS. Plates were counted using a TopCount reader, and data were analyzed using proprietary software.

Checkpoint Abrogation Assay.^{6a} HT29 cells (3 × 10⁵) were seeded in 96-well plates and incubated overnight. Cells were treated for 2 h with camptothecin (topoisomerase I inhibitor, 0.07 μg/mL) to induce the G₂ checkpoint. Cells were then treated for 20 h with vehicle (0.5% DMSO) or caffeine (4 mmol/L, positive control) plus nocodazole (1 μg/mL) or a 12-point titration of **4** (12.5 μmol/L to 6 nmol/L) plus nocodazole. Nocodazole alone-treated cells with no camptothecin pretreatment were used to determine the maximum mitotic index. Cells were fixed with 3.7% formaldehyde for 1 h, permeabilized with PBS containing 0.05% Triton X, and incubated with anti-pH3 antibody for 2 h followed by Alexa Fluor 488 anti-rabbit (Molecular Probes) and Hoechst stain for 1 h. Mitotic index was determined on the ArrayScan and expressed as the percentage of cells undergoing mitosis. The EC₅₀ was calculated by concentration–response curve fitting using three-variable logistical equations within

XLfit (model 205) with the curve bottom constrained to 0 and the top constrained to 100 by nocodazole alone treatment.

In Vivo Studies. In vivo studies are described in detail in ref 6a cited in this report.

Overexpression and Purification of JNK1 Kinase. An N-terminally truncated form of JNK1 (9-364) was expressed in TOP10 *E. coli* cells, making use of the expression plasmid pBADHisA resulting in an expression construct bearing an N-terminal His-tag for purification ease that can be removed via thrombin cleavage. Expression was started at 28 °C at an OD₆₀₀ of around 0.8 by addition of 0.2% (w/v) arabinose. The cells were harvested by centrifugation 6–18 h after induction, and the pellets were stored at –80 °C. A pellet corresponding to 1 L of culture was suspended in 100 mL of ice-cold lysis buffer (50 mM Tris/HCl, pH 7.5, 500 mM NaCl, 10 mM imidazole, 10% glycerol, 1 mM DTT). After cell breakage through ultrasonication, cell debris was removed by centrifugation and the supernatant was collected. Then 10 mL of Ni²⁺-NTA Superflow resin (Qiagen) equilibrated in lysis buffer was added to the cleared lysate and incubated for 1 h at 4 °C on a shaking platform. The matrix was washed with 75–150 mL of lysis buffer, and JNK1 protein was eluted with 25 mL of elution buffer (50 mM Tris/HCl, pH 7.5, 500 mM NaCl, 300 mM imidazole, 10% glycerol, and 1 mM DTT). After overnight dialysis at 4 °C against 2 L of 50 mM Tris/HCl, pH 7.5, 500 mM NaCl, 10 mM imidazole, 10% glycerol, 1 mM DTT, the His-tag was released by thrombin treatment (Pharmacia, 10 U/mg target protein) for 2 h and passed over a Ni²⁺-NTA column (Qiagen, 10 mL column volume) in the same buffer. The flow-through was collected, concentrated to about 8–10 mL, and applied directly onto a Superdex75 XK26/60 column (2 mL/min flow rate) equilibrated with 25 mM Tris/HCl, pH 7.5, 150 mM NaCl, 10% glycerol, 2 mM DTT at 12 °C. Fractions of pure JNK1 eluting at around 160 mL retention volume were pooled and concentrated to 9.5 mg/mL while exchanging into a storage buffer consisting of 25 mM HEPES, pH 7.0, plus 5 mM DTT. The final yield was typically in the range of 80–120 mg/L.

Crystallization, Ligand Soaking, and Structure Determination of 1 in Complex with JNK1. Crystals of JNK1 kinase were grown using the hanging-drop vapor diffusion method with a reservoir containing 15% PEG2000 MME, 100 mM HEPES, pH 7, and 10 mM DTT and 1 mM AMP-PNP. Crystals were soaked for 24 h in mother liquor containing 5 mM **1** and 10% DMSO. Data were collected at beamline 711, MAX Lab, Lund, Sweden, at 100 K. The data were processed with MOSFLM¹⁵ and programs in the CCP4 suite.¹⁶ Refinement and model rebuilding were carried out using CNX,¹⁷ Autobuster,¹⁸ and COOT.¹⁹

Overexpression and Purification of CHK1 Kinase. Checkpoint kinase (residues 1–276 and 1–289) protein production was as previously described.¹⁴

Cocrystallization CHK1 in Complex with 2, 3, and 4. Cocrystals of **2** in complex with CHK1 kinase (1–289) and **3b** and **4** in complex with CHK1 kinase (1–276) were prepared as previously described.¹⁴

Data Collection and Structure Solution of CHK1 Kinase Complexes. Diffraction data for the CHK1–**2** complex were collected at Daresbury on beamline PX9.6 equipped with an ADSC Quantum 4 detector, using a Si111 monochromatic wavelength of 0.86 Å at 100 K. Diffraction data for the CHK1–**3b** complex were collected at the ESRF on beamline ID14-4 equipped with an ADSC CCD detector, using a Si111 monochromatic wavelength of 1.0052 Å. Diffraction data for the CHK1–**4** complex were collected on a Rigaku MM007 rotating anode X-ray generator equipped with a Saturn 92 CCD detector, using Osmic Varimax HF mirrors and Cu Kα radiation. Data for the CHK1–**2**, and CHK1–**3b** complexes were processed using MOSFLM¹⁵ and were scaled, merged, and reduced using CCP4 software.¹⁶ Data for CHK1–**4** complex were processed using d*trek.²⁰ The structures were solved by molecular replacement using coordinates of the CHK1 kinase domain as a trial model using CCP4 software.¹⁶ Protein and inhibitor were modeled into the electron density using Quanta,²¹ COOT,¹⁹ and Flynn.²⁴ The models were refined using CNX¹⁷ and the CCP4 program Refmac5.²³

Table 5. Crystallographic Data Collection and Refinement Statistics for Complexes of 1 with c-Jun NH₂-Terminal Kinase 1 and for 2, 3b, and 4 with Checkpoint Kinase 1

parameter	1	2	3b	4
PDB code	3PZE	2YDI	2YDJ	2YDK
protein	JNK1	CHK1	CHK1	CHK1
space group	<i>P</i> 2 ₁ 2 ₁ 2 ₁	<i>P</i> 2 ₁	<i>P</i> 2 ₁ 2 ₁ 2 ₁	<i>P</i> 2 ₁
cell <i>a</i> , <i>b</i> , <i>c</i> (Å)	49.5, 71.3, 106.7	45.1, 66.0, 58.2,	41.6, 70.8, 104.1	42.0, 64.9, 120,
cell β (deg)		93.8		98.8
resolution limit (Å)	32.3–2.0 (2.11–2.0)	37.2–1.6 (1.69–1.6)	23.9–1.9 (2.0–1.9)	43.8–1.85 (1.92–1.85)
completeness (%)	96.7 (94.7)	87.6 (39.7)	94.92 (83.8)	84.4 (78.7)
reflections, unique	25419	39316	23512	46087
multiplicity	3.5 (3.5)	2.2 (1.2)	2.39 (2.1)	2.44 (2.35)
<i>R</i> _{merge} (%)	0.096 (0.83)	0.052 (0.20)	0.076 (0.38)	0.089 (0.39)
<i>I</i> / σ (<i>I</i>)	8.0 (1.5)	6.2 (4.0)	5.9 (2)	5.8 (2.2)
final <i>R</i> for all reflections (work/free) (%)	20.4/24.0	16.7/20.1	18.1/22.6	22.8/27.4
no. of atoms: protein/ligand/solvent	2817/18/197	2216/24/332	2118/24/292	4114/50/414
rmsd values				
bond length (Å)	0.010	0.010	0.012	0.01
bond angle (deg)	1.12	1.27	1.37	1.24
temp factors				
protein (Å ²)	36.5	21.9	28.3	30.5
ligand (Å ²)	45.7	30.0	24.9	27.3
solvent (Å ²)	42.7	35.4	37.7	39.1
Ramachandran plot ^a				
most favored (%)	96.8	91.4	89.1	90
additional allowed (%)	2.9	8.6	9.6	9
generously allowed (%)	0	0	0.9	0.8
disallowed (%)	0.3	0	0.4	0.2

^aPercentage of residues in regions of the Ramachandran plot, according to PROCHECK.²⁵ Numbers in parentheses refer to the highest resolution shell.

Atomic coordinates and structure factors for the JNK1 complex with compound 1 and the CHK1 complexes with compounds 2, 3b, and 4 have been deposited in the Protein Data Bank (PDB codes 3PZE, 2YDI, 2YDJ, and 2YDK, respectively) together with structure factors and detailed experimental conditions. Crystallographic statistics for the data processing and refinement are shown in Table 5.

AUTHOR INFORMATION

Corresponding Author

*Phone: +1 978-394-3088. E-mail: vibha.oza@gmail.com.

Present Addresses

[†]Department of Biochemistry and Molecular Biophysics, Washington University School of Medicine, 660 S. Euclid Avenue, Box 8231, St. Louis, MO 63110, United States.

[#]756 Central Park Drive West, 235, Plainfield, IN 46168, United States.

[∞]AstraZeneca-MedImmune, One MedImmune Way, Gaithersburg, MD 20878, United States.

[×]AstraZeneca-Innovation Center China (ICC), 898 Halei Road, Zhangjiang Hi-Tech Park, Pudong New Area 201203, China.

[○]Eleven Cobble Court, Unionville, Connecticut, CT 06085, United States.

[●]4310 Trias Street, San Diego, CA 92103, United States.

Notes

The authors declare no competing financial interest.

ACKNOWLEDGMENTS

The authors thank Stefan Geschwindner for the data on JNK1, Anne White and Anna Valentine for protein production, and Tina Howard for crystallization support. The authors also thank

Julie Tucker and Richard Pauptit for their critical evaluation of this manuscript.

ABBREVIATIONS USED

APCI, atmospheric pressure chemical ionization; ATP, adenosine 5-triphosphate; CDCl₃, deuterated chloroform; CI, chemical ionization; CYP450, cytochrome P450; EI, electron impact; ESP, electrospray; GST, glutathione S-transferase; IHC, immunohistochemistry; iv, intravenous; LC, liquid chromatography; PHH3, phosphohistone H3; TMS, tetramethylsilane; HTS, high throughput screen; TCU, thiophenecarboxamide urea; 2-TCU, 2-uriedothiophenecarboxamide urea; 3-TCU, 3-uriedothiophenecarboxamide urea; DMSO, dimethylsulfoxide; EtOAc, ethyl acetate; DCM, dichloromethane; DTT, dithiothriol; HEPES, 4-(2-hydroxyethyl)-1-piperazineethanesulfonic acid; THF, tetrahydrofuran; Rochelle's salt, sodium potassium tartrate; MgSO₄, magnesium sulfate

REFERENCES

- (1) (a) Russell, K. J.; Wiens, L. W.; Demers, G. W.; Galloway, D. A.; Plon, S. E.; Gondine, M. Abrogation of the G2 checkpoint results in differential radiosensitization of G1 checkpoint-deficient and G1 checkpoint-competent cells. *Cancer Res.* **1995**, *55*, 1639–1642. (b) Wang, Q.; Fan, S.; Eastman, A.; Worland, P. J.; Sausville, E. A.; O'Connor, P. M. UCN-01: a potent abrogator of G2 checkpoint function in cancer cells disrupted with p53. *J. Natl. Cancer Inst.* **1996**, *88*, 956–965. (c) Graves, P. R.; Yu, L.; Schwarz, J. K.; Gales, J. The CHK1 protein kinase and the Cdc25C regulatory pathways are targets of the anticancer agent UCN-01. *J. Biol. Chem.* **2000**, *275*, S600–S605. (d) Busby, E. C.; Leistriz, D. F.; Abraham, R. T.; Karnitz, L. M.; Sarkaria, J. N. The radiosensitizing agent 7-hydroxystaurosporine (UCN-01) inhibits the DNA damage checkpoint kinase hCHK1.

- Cancer Res.* **2000**, *60*, 2108–2012. (e) Koniaras, K.; Cuddihy, A. R.; Christopoulos, H.; Hogg, A.; O'Connell, M. J. Inhibition of CHK1-dependent G2 DNA damage checkpoint radiosensitizes p53 mutant human cells. *Oncogene* **2001**, *20*, 7453–7463. (f) Luo, Y.; Rockow-Magnone, S. K.; Joseph, M. K. Abrogation of G2 checkpoint specifically sensitize p53 defective cells to cancer chemotherapeutic agents. *Anticancer Res.* **2001**, 2123–2128. (g) Luo, Y.; Rockow-Magnone, S. K.; Kroeger, P. E. Blocking CHK1 expression induces apoptosis and abrogates the G2 checkpoint mechanism. *Neoplasia* **2001**, *3*, 411–419. (h) Zhao, H.; Watkins, J. L.; Piwnica-Worms, H. Disruption of the checkpoint kinase 1/cell division cycle 25A pathway abrogates ionizing radiation induced S and G2 checkpoints. *Proc. Natl. Acad. Sci. U.S.A.* **2002**, *99*, 14795–14800. (i) Chen, Z.; Xiao, Z.; Chen, J. Human CHK1 expression is dispensable for somatic cell death and critical for sustaining G2 DNA damage checkpoint. *Mol. Cancer Ther.* **2003**, *2*, 543–548.
- (2) (a) Lau, C. C.; Pardee, A. B. Mechanism by which caffeine potentiates lethality of nitrogen mustard. *Proc. Natl. Acad. Sci. U.S.A.* **1982**, *79*, 2942–2946. (b) Musk, S. R.; Steel, G. G. Override of the radiation-induced mitotic block in human tumor cells by methylxanthines and its relationship to the potentiation of cytotoxicity. *Int. J. Radiat. Biol.* **1990**, *57*, 1105–1112. (c) Teicher, B. A.; Holden, S. A.; Herman, T. S.; Epelbaum, R.; Pardee, A. B.; Dezube, B., Jr. Efficacy of pentoxifylline as a modulator of alkylating agent activity in vitro and in vivo. *Anticancer Res.* **1991**, *11*, 1555–1560. (d) Pan, Y.; Ren, K. H.; He, H. W.; Shao, R. G. Knockdown of CHK1 sensitizes human colon carcinoma HCT116 cells in a p53-dependent manner to lidamycin through abrogation of a G2/M checkpoint and induction of apoptosis. *Cancer Biol. Ther.* **2009**, *8*, 1559–1566.
- (3) (a) Ashwell, S.; Janetka, J. W.; Zabludoff, S. D. Keeping checkpoint kinases in line: new selective inhibitors in clinical trials. *Expert Opin. Invest. Drugs* **2008**, *17* (9), 1331–1340. (b) Janetka, J.; Almeida, L.; Ashwell, S.; Brassil, P.; Daly, K.; Deng, C.; Gero, T.; Glynn, R.; Horn, C.; Ioannidis, S.; Lyne, P.; Newcombe, N. J.; Oza, V. B.; Pass, M.; Springer, S. K.; Su, M.; Toader, D.; Vasbinder, M. M.; Yu, D.; Yu, Y.; Zabludoff, S. D. Discovery of a novel class of 2-ureido thiophene carboxamide checkpoint kinase inhibitors. *Bioorg. Med. Chem. Lett.* **2008**, *18*, 4242–4248. (c) Janetka, J.; Ashwell, S.; Zabludoff, S. D. *Expert Opin. Ther. Pat.* **2009**, *19*, 165–197. (d) Ashwell, S.; Zabludoff, S. *Clin. Cancer Res.* **2008**, *14*, 4032. (e) Oza, V.; Ashwell, S.; Brassil, P.; Breed, J.; Deng, C.; Ezhuthachan, J.; Haye, H.; Horn, C.; Janetka, J.; Lyne, P.; Newcombe, N.; Otterbien, L.; Pass, M.; Read, J.; Rowsell, S.; Su, M.; Toader, D.; Yu, D.; Yu, Y.; Valentine, A.; Webborn, P.; White, A.; Zabludoff, S.; Zheng, X. Discovery of a novel class of triazolones as checkpoint kinase inhibitors: hit to lead exploration. *Bioorg. Med. Chem. Lett.* **2010**, *20*, 5133–5138. (f) Zhao, L.; Zhang, Y.; Dai, C.; Guzi, T.; Wiswell, D.; Seghezzi, W.; Parry, D.; Fischmann, T.; Siddiqui, M. A. Design, synthesis and SAR of thienopyridines as potent CHK1 inhibitors. *Bioorg. Med. Chem. Lett.* **2010**, *20*, 7216–7221. (g) Yuki, S.; Ichikawa, S.; Osada, A.; Matsuda, A. Synthesis and evaluation of 5-substituted 9-hydroxypyrrrolo[3,4-c]carbazole-1,3(2H,6H)-diones as check point 1 kinase inhibitors. *Bioorg. Med. Chem.* **2010**, *18*, 7878–7889. (h) Walton, M. I.; Eve, P. D.; Hayes, A.; Valenti, M.; De Haven, B. A.; Box, G.; Boxall, K. J.; Aherne, G. W.; Eccles, S. A.; Raynaud, F. I.; Williams, D. H.; Reader, J. C.; Collins, I.; Garrett, M. D. The preclinical pharmacology and therapeutic activity of the novel CHK1 inhibitor SAR-020106. *Mol. Cancer Ther.* **2010**, *9*, 89–100. (i) Hong, P. C.; Chen, L. J.; Lai, T. Y.; Yang, H. Y.; Chiang, S. J.; Lu, Y. Y.; Tsai, P. K.; Hsu, H. Y.; Wei, W. Y.; Liao, C. B. Synthesis of selenophene derivatives as novel CHK1 inhibitors. *Bioorg. Med. Chem. Lett.* **2010**, *20*, 5065–5068. (j) Drobnick, J.; Appleton, B.; Axford, L.; Beresini, M.; Burton, B.; Chen, H.; Clark, D.; Clark, K.; Crackett, P.; Ellwood, C.; Gancia, E.; Ganguli, A.; Gill, M.; Goldstein, J.; Goodacre, S.; Hewitt, J.; Hurst, D.; Kintz, S.; Lockey, P.; Lyssikatos, J.; Major, S.; McLeod, C.; McNair, D.; Medard, G.; Narukulla, R.; Newman, R.; Sideris, S.; Weismann, C.; Hunt, H.; Williams, K.; Malek, S.; Gazzard, L. *Abstracts of Papers*, 240th National Meeting of the American Chemical Society, Boston, MA, U.S., August 22–26, 2010; American Chemical Society: Washington, DC, 2010. (k) Matthews, T. P.; McHardy, T.; Klair, S.; Boxall, K.; Fisher, M.; Cherry, M.; Allen, C. E.; Addison, G. J.; Ellard, J.; Aherne, G. W.; Westwood, I. M.; Van Montfort, R.; Garrett, M. D.; Reader, J. C.; Collins, I. Design and evaluation of 3,6-di(hetero)aryl imidazo[1,2-a]pyrazines as inhibitors of checkpoint and other kinases. *Bioorg. Med. Chem. Lett.* **2010**, *20*, 4045–4049. (l) Fiumana, A.; Bedford, S.; Borgognoni, J.; Drysdale, M.; Foloppe, N.; Jordan, A. M.; Massey, A.; Stokes, S.; Web, P. *Abstracts of Papers*, 239th National Meeting of the American Chemical Society, San Francisco, CA, U.S., March 21–25, 2010; American Chemical Society: Washington, DC, 2010; MEDI-143. (m) Blasina, A.; Hallin, J.; Chen, E.; Arango, M.; Kraynov, E.; Register, J.; Grant, S.; Ninkovic, S.; Chen, P.; Nichols, T.; O'Connor, P.; Anderes, K. Breaching the DNA damage checkpoint via PF-00477736, a novel small-molecule inhibitor of checkpoint kinase 1. *Mol. Cancer Ther.* **2008**, *7*, 2394–2404. (n) Laichbury, M.; Collins, I. *Expert Opin. Ther. Pat.* **2011**, *21*, 1191–1210 (also refer to www.clinicaltrials.gov).
- (4) Baxter, A.; Brough, S.; Cooper, A.; Floettmann, E.; Foster, S.; Harding, C.; Kettle, J.; McNally, T.; Martin, C.; Mobbs, M.; Needham, M.; Newham, P.; Paine, S.; St-Gallay, S.; Salter, S.; Unitt, J.; Xue, Y. Hit-to-lead studies: the discovery of potent, orally active, thiophene-carboxamide IKK-2 inhibitors. *Bioorg. Med. Chem. Lett.* **2008**, *18*, 4242–4248.
- (5) Lyne, P. D.; Kenny, P. W.; Cosgrove, D. A.; Deng, C.; Zabludoff, S.; Wendoloski, J. J.; Ashwell, S. Identification of compounds with nanomolar binding affinity for checkpoint kinase-1 using knowledge-based virtual screening. *J. Med. Chem.* **2004**, *47*, 1962.
- (6) (a) Zabludoff, S.; Deng, C.; Grondine, M.; Sheehy, A.; Ashwell, S.; Caleb, B.; Green, S.; Haye, H.; Horn, C.; Janetka, J.; Liu, D.; Mouchet, E.; Ready, S.; Rosenthal, J.; Queva, C.; Schwartz, G. K.; Taylor, K. J.; Tse, A. N.; Walker, G. E.; White, Anne, M. AZD7762, a novel checkpoint kinase inhibitor, drives checkpoint abrogation and potentiates DNA-targeted therapies. *Mol. Cancer Ther.* **2008**, *7*, 9. (b) Ashwell, S. *Abstracts of Papers*, 2007 AACR Annual Meeting, Los Angeles, CA, April 14–18, 2007; AACR: Philadelphia, PA, 2007. (c) Almeida, L.; Ashwell, S.; Ayres, D. W.; Brassil, P. J.; Daly, K.; Deng, C.; Gero, T.; Glynn, R. E.; Horn, C. L.; Ioannidis, S.; Janetka, J. W.; Lyne, P.; Oza, V. B.; Springer, S. K.; Su, M.; Toader, D.; Vasbinder, M. M.; Yu, D.; Yu, Y.; Zabludoff, S. D. *Abstracts of Papers*, 2007 EORTC-NCI-AACR International Meeting on Molecular Targets and Therapeutics, San Francisco, CA, October 22–26, 2007; EORTC-NCI-AACR, 2007; p A233. (d) Mitchell, J. B.; Choudhuri, R.; Fabre, K.; Sowers, A. L.; Citrin, D.; Zabludoff, S. D.; Cook, J. A. In vitro and in vivo radiation sensitization of human tumor cells by a novel checkpoint kinase inhibitor, AZD7762. *Clin. Cancer Res.* **2010**, *16*, 2076–208. (e) Ashwell, S.; Caleb, B. L.; Green, S.; Grondine, M. R.; Haye, H. R.; Horn, C. L.; Janetka, J. W.; Liu, D.; Mouchet, E.; Ready, S.; Rosenthal, J. L.; Queva, C.; Taylor, K. J.; Sheehy, A. M.; Walker, G. E.; White, A. M.; Zabludoff, S. D. *Abstracts of Papers*, 2007 EORTC-NCI-AACR, International Meeting on Molecular Targets and Therapeutics, San Francisco, CA, October 22–26, 2007; EORTC-NCI-AACR, 2007; p A232.
- (7) (a) Buchstaller, H. P.; Siebert, C. D.; Lyssy, R. H.; Frank, I.; Duran, A.; Gottschlich, R.; Noe, C. R. Synthesis of novel 2-aminothiophene-3-carboxylates by variations of the Gewald reaction. *Monatsh. Chem.* **2001**, *132*, 279–293. (b) Sabnis, R. W.; Rangnekar, D. W.; Sonawane, N. D. 2-Aminothiophenes by the Gewald reaction. *J. Heterocycl. Chem.* **1999**, *36*, 333–345.
- (8) Málek, J. Reductions by metal alkoxaluminum hydrides. Part II. Carboxylic acids and derivatives. *Nitrogen Compd., Sulfur Compd. Org. React.* **1988**, 249–590.
- (9) (a) Levin, J. I.; Turos, E.; Weinreb, S. M. An alternative procedure for the aluminum-mediated conversion of esters to amides. *Synth. Commun.* **1982**, *13*, 989–993. (b) Lipton, M. F.; Basha, A.; Weinreb, S. M. *Org. Synth.* **1980**, 59, 49.
- (10) (a) A select subset of these compounds was previously disclosed in ref 3b by Janetka et al. (b) Topliss, J.; Yudis, M. P-Substituent constants for the 2H-1,2,4-benzothiadiazine 1,1-dioxide system. *J. Med. Chem.* **1972**, *15*, 394–400.

(11) Morgan, M. A.; Parsels, L. A.; Parcels, J. D.; Mesiwalal, A. K.; Maybaum, J.; Lawrence, T. S. Role of checkpoint kinase 1 in preventing premature mitosis in response to gemcitabine. *Cancer Res.* **2005**, *65*, 6835–6842.

(12) Karnitz, L. M.; Flatten, K. S.; Wagner, J. M. Gemcitabine induced activation of checkpoint signaling pathways that affect tumor cell survival. *Mol. Pharmacol.* **2005**, *68*, 1636–1644.

(13) For data on sensitization to radiation therapy in the presence of AZD7762, refer to ref 6d. For cloning, sequencing, overexpression, purification, and crystallization of CHK1 kinase, refer to ref 3e.

(14) Ma, C. X.; Janetka, J. W.; Piwnica-Worms, H. Death by releasing the breaks: CHK1 inhibitors as cancer therapeutics. *Trends Mol. Med.* **2011**, *17*, 88–96.

(15) Leslie, A. G. W. Mosflm. *Jt. CCP4 + ESF-EAMCB Newsl. Protein Crystallogr.* **1992**, *26*.

(16) The CCP4 suite: programs for protein crystallography. *Acta Crystallogr.* **1994**, *D50*, 760–763.

(17) CNX, version 2000.1; Accelrys: San Diego, CA.

(18) Bricogne, G.; Blanc, E.; Brandl, M.; Flensburg, C.; Keller, P.; Paciorek, W.; Roversi, P.; Smart, O. S.; Vonnrhein, C.; Womack, T. O. *Autobuster*, version 2.8.0; Global Phasing Ltd.: Cambridge, U.K., 2009.

(19) Emsley, P.; Cowtan, K. Coot: model-building tools for molecular graphics. *Acta Crystallogr.* **2004**, *D60*, 2126–2132.

(20) Pflugrath, J. W. d*trek: the finer things in X-ray diffraction data collection. *Acta Crystallogr.* **1999**, *D55*, 1718–1725.

(21) *Quanta: QUANTA2000*; Accelrys: San Diego, CA.

(22) DeLano, W. L. *Pymol: The PyMOL Molecular Graphics System*; DeLano Scientific: San Carlos, CA, U.S., 2002; <http://www.pymol.org>.

(23) Murshudov, G. N.; Vagin, A. A.; Dodson, E. J. Refmac: refinement of macromolecular structures by the maximum-likelihood method. *Acta Crystallogr.* **1997**, *D53*, 240–255.

(24) *Flynn*, version 1.1.1; OpenEye Scientific Software, Inc.: Santa Fe, NM, U.S., 2010; www.eyesopen.com.

(25) Laskowski, R. A.; MacArthur, M. W.; Moss, D. S.; Thornton, J. M. PROCHECK, a program to check the stereochemical quality of protein structures. *J. Appl. Crystallogr.* **1993**, *26*, 283–291.